

Three-wave mixing in conjugated polymer solutions: Two-photon absorption in polydiacetylenes

R. R. Chance and M. L. Shand

Corporate Research Center, Allied Chemical Corporation, Morristown, New Jersey 07960

C. Hogg and R. Silbey

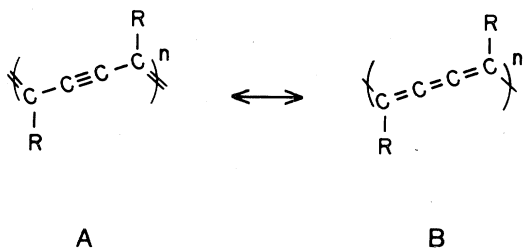
Department of Chemistry, Massachusetts Institute of Technology, Cambridge, Massachusetts 02139

(Received 22 May 1980)

Three-wave-mixing spectroscopy is used to determine the dispersive and absorptive parts of a strongly allowed two-photon transition in a series of polydiacetylene solutions. The data analysis yields the energy, width, symmetry assignment, and oscillator strength for the two-photon transition. The data conclusively demonstrate that strong two-photon absorption is a fundamental property of the polydiacetylene backbone. The remarkably large two-photon absorption coefficients are explained by large oscillator strengths for both transitions involved in the two-photon absorption combined with strong one-photon resonance effects. The experimental results are shown to be consistent with a simple theoretical model for the energies and oscillator strengths of the one- and two-photon-allowed transitions.

I. INTRODUCTION

The linear and nonlinear optical properties of polydiacetylenes have received considerable attention recently.¹⁻³ This interest is attributable to the fully-conjugated backbone structure

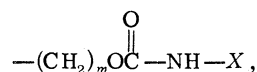


which leads to essentially one dimensional electronic properties. The acetylene mesomer (A) is the lowest-energy conformation for the polymer, and numerous x-ray structures have yielded bonding sequences which are very close to A above.⁴ There is some evidence for the higher-energy butatriene mesomer^{5,6} in systems, such as the ones we are considering here, where backbone strain is introduced due to intramolecular interactions of the substituent groups (R).

Extensive electron delocalization along the chain direction leads to an electronic transition energy for one-photon absorption (E_0) of typically 15 000–16 000 cm^{-1} for an unstrained backbone.⁷ This value is very close to that of polyacetylene (or polyene) $(\text{HC}=\text{CH})_n$ which has $E_0 \sim 15\,000\text{ cm}^{-1}$.⁸ For both polymers, E_0 varies with chain length (or conjugation length) in much the same manner.⁹ This analogy to the polyene system leads to the expectation that the polydiacetylenes might have unusually large third-order susceptibilities (χ) as

had been demonstrated for polyenes of varying length. This expectation was borne out by the work of Sauteret *et al.*¹ who found χ values for polydiacetylene crystals which were comparable to those of inorganic semiconductors. Their results suggested attractive possibilities for these one-dimensional materials in nonlinear optical devices. Applications in parametric oscillators which utilize three-wave mixing were particularly attractive. However, three-wave-mixing experiments were unsuccessful due to phase-matching problems,¹⁰ as well as nonlinear absorption problems which Lequime and Hermann¹¹ attributed to absorption by photogenerated defects.

Recently, polydiacetylenes have been discovered which are soluble in common organic solvents.¹² These polymers have urethane substituent groups of the form



where $m = 3$ or 4. The polymers considered in this paper have $X = -\text{COOC}_4\text{H}_9$ and are referred to as m BCMU (BCMU = butoxycarbonylmethylurethane). The most interesting feature of these polymers is that the visible absorption spectra can be varied in a controlled manner by solvent variation (see Fig. 1). This phenomenon is due to the fact that the degree of conjugation (or planarity) of the chains in solution is controlled by intramolecular hydrogen bonding of the C=O and N-H functionalities on adjacent urethane substituent groups. In good solvents, such as CHCl_3 , about one out of every four polymer repeat units (r.u.) is not hydrogen bonded, which leads to a conjugation length of ~ 4 r.u. and a large blue shift in optical absorption ($E_0 \sim 21\,000\text{ cm}^{-1}$).¹² In poor solvents, such as CHCl_3 -hexane mixtures,

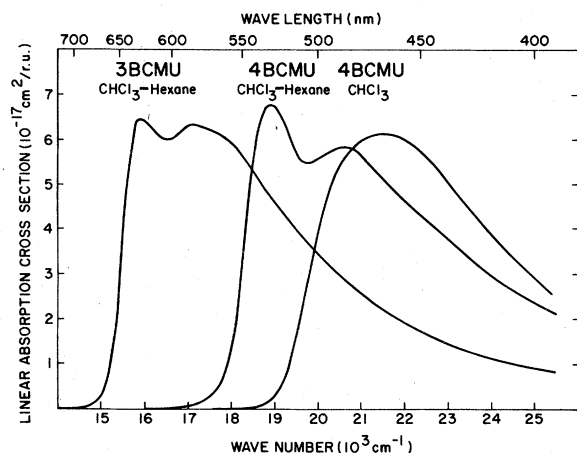


FIG. 1. Linear absorption spectra for polydiacetylene solutions. The three solutions are referred to in the text as "blue," "red," and "yellow" (from left to right in the figure).

essentially every polymer unit is hydrogen bonded, which leads to $E_0 \sim 15900 \text{ cm}^{-1}$ for 3BCMU and $E_0 \sim 18900 \text{ cm}^{-1}$ for 4BCMU. The blue shift of the latter compared to the usual crystal values is attributed to strain.^{12,13} It is systems such as 4BCMU which have indicated butatriene backbones in single-crystal studies.⁵

We have undertaken an investigation of three-wave mixing (3WM)¹⁴⁻¹⁹ in *m*BCMU solutions because of their dramatic variation in linear optical properties with solvent variation and because of the elimination of the possibility of any photo-generated defect absorption, which has been suggested as a problem in two-photon experiments in crystals.¹¹ We find that the nonlinear optical properties of these solutions are completely dominated by remarkably strong two-photon absorption. Experimental details are given in Sec. II. The results for two-photon hyperpolarizabilities of these solutions are presented in Sec. III. A brief theoretical discussion of these results in terms of a simple Hückel model is presented in Sec. IV. In Sec. V, we consider application possibilities and discuss our results in comparison to previous results with polydiacetylene crystals. A preliminary report of this work has appeared recently.²⁰

II. EXPERIMENTAL

The 3WM apparatus has been described elsewhere.²¹ 3WM is accomplished by focusing two laser beams with frequencies ω_1 and ω_2 in the polymer solution. Incident laser beams are generated by two dye lasers pumped by a single N_2 laser. Wavelengths for the incident beams ranged from 760 to 590 nm (or to the region of large absorption). The beams are focused into

the sample with a 15-cm focal length lens. The crossing angle between the two beams is adjusted for phase matching (approximately 4° outside the sample cell). The sample solutions are held in a 1-cm cuvette. The beam generated at $\omega_3 = 2\omega_1 - \omega_2$ is filtered with a double monochromator and its intensity measured with a photomultiplier and boxcar electronics. Our analysis utilizes the measurement of the ω_3 intensity as a function of polymer concentration in the determination of the real and imaginary parts of the two-photon hyperpolarizability.^{20,21}

In order to extend the range of $2\omega_1$ possible with a limited range of laser excitation, both CARS (coherent anti-Stokes Raman scattering) and CSRS (coherent Stokes Raman scattering) are used. In both cases $\omega_3 = 2\omega_1 - \omega_2$. In the CARS mode $\omega_3 > \omega_1 > \omega_2$; in the CSRS mode $\omega_2 > \omega_1 > \omega_3$. One-photon resonance effects are the same in both cases as described later. Phase matching is also the same in both cases with $\vec{k}_3 = 2\vec{k}_1 - \vec{k}_2$.

Materials preparation has been described previously,¹² as have the linear optical properties of these materials in solution,¹² in crystalline phase,⁷ and in solution cast films.⁷ Linear absorption spectra for the three solutions considered herein are given in Fig. 1. These solutions are referred to in the text as "yellow": 4BCMU in CHCl_3 , "red": 4BCMU in 1:2 CHCl_3 -hexane mixture, and "blue": 3BCMU in 1:1 CHCl_3 -hexane mixture. The concentration range in the yellow solution is $0-120 \times 10^{17} \text{ r.u./cm}^3$. For the other solutions an upper limit is imposed on the concentration range due to polymer precipitation: $\sim 4 \times 10^{17} \text{ r.u./cm}^3$ for the red solution and $\sim 9 \times 10^{17} \text{ r.u./cm}^3$ for the blue solution.¹²

III. RESULTS

The two-photon hyperpolarizability is determined from the variation of the ω_3 intensity with polymer concentration. The maximum accessible polymer concentration is determined by the precipitation (cloud) point, which is largest for the yellow solution. Therefore, the concentration dependence is determined most accurately for the yellow solution. In addition, the low-energy tail of the linear absorption (which corresponds to the high-frequency cut off of our experimental range) is at higher energies in the yellow solution than in the blue or red solutions. Therefore, the yellow solutions yield the more extensive data sets and these results are presented and discussed first.

Six samples of yellow solution were prepared with various concentrations up to 1.2×10^{19}

r.u./cm³. Higher concentrations are available. However, at higher concentrations and in regions of linear absorption the phase-matching conditions depend on concentration. These higher concentrations are not used in order to avoid changing the phase-matching angle during a series of measurements. The third-order nonlinear mixing is determined in both the CARS and CSRS geometries. $\omega_1 - \omega_2$ is tuned away from any Raman resonances at about 1300 cm⁻¹. (A CARS study of Raman resonances in these solutions has been previously reported.²¹) The output intensity is measured for each sample and for the solvent without polymer (pure chloroform for the yellow solution). The total susceptibility is

$$\chi_{\text{tot}} = \chi_s + \chi_p + \chi_T = \chi_s + N\gamma_p + N(\gamma'_T + \gamma''_T), \quad (1)$$

where χ_s is the solvent susceptibility (assumed to be positive and real), χ_p is the polymer non-resonant susceptibility, χ_T is the two-photon susceptibility, N is the polymer concentration, γ_p is the polymer nonresonant hyperpolarizability, and $\gamma_T = \gamma'_T + i\gamma''_T$ is the two-photon hyperpolarizability. (Note that we take $\gamma = \chi/N$, ignoring local-field effects.²⁰) The ω_3 intensity I is proportional to $|\chi|^2$ so that

$$\frac{I^{s+p}}{I^s} = \frac{|\chi_{\text{tot}}|^2}{|\chi_s|^2} = 1 + \frac{2NR}{\chi_s} + \frac{N^2(R^2 + \gamma_T'^2)}{\chi_s^2}, \quad (2)$$

where I^{s+p} is the ω_3 intensity for the polymer solution, I^s is the ω_3 intensity for the pure solvent, and $R = \gamma_p + \gamma'_T$. It has been shown previously that the contribution of γ_p to R is very small over our frequency range.²¹ Therefore, R can be identified as the real part of the two-photon hyperpolarizability γ'_T .

I^{s+p}/I^s as a function of N is shown in Fig. 2 for two values of ω_1 . The closed and open circles are the data with $2\omega_1 = 32\,362$ cm⁻¹ and $26\,554$ cm⁻¹, respectively. For the former, the intensity decreases with increasing N for small N , which indicates $\gamma'_T < 0$ for $2\omega_1 = 32\,362$ cm⁻¹; for the latter, the intensity increases with increasing N indicating $\gamma'_T > 0$ for $2\omega_1 = 26\,554$ cm⁻¹. Thus, the energy of the two-photon state, determined by $\gamma'_T = 0$, is between these two values of $2\omega_1$. The solid lines in Fig. 2 are obtained from Eq. (2) with γ'_T/χ_s and γ''_T/χ_s determined from a linear regression analysis of

$$\frac{(I^{s+p}/I^s - 1)}{N} = \frac{2\gamma'_T}{\chi_s} + N \left[\left(\frac{\gamma'_T}{\chi_s} \right)^2 + \left(\frac{\gamma''_T}{\chi_s} \right)^2 \right]. \quad (3)$$

The analysis also determined a range of γ'_T/χ_s and γ''_T/χ_s with a 90%-confidence limit. The χ_s values are taken from Ref. 17: $\chi_s = 0.87 \times 10^{-14}$ esu for CHCl₃ and $\chi_s = 1.06 \times 10^{-14}$ esu for hexane. There are no two-photon resonances in the sol-

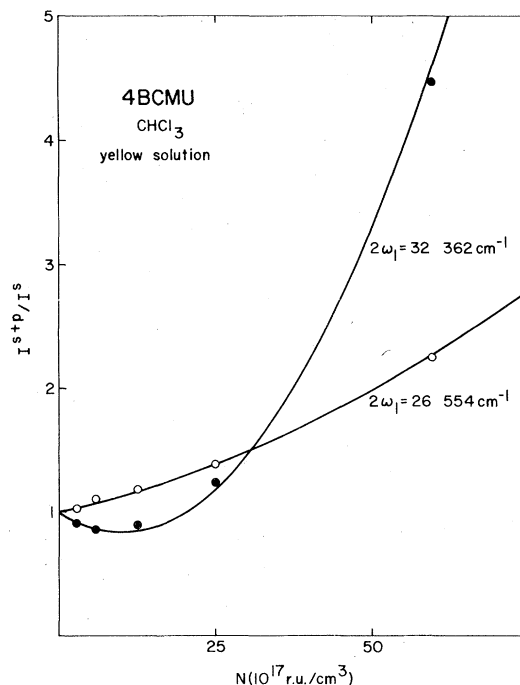


FIG. 2. Variation in the normalized ω_3 output intensity with polymer concentration for the yellow solution. The solid lines represent theoretical fits to the data according to Eq. (3).

vents in the frequency range of interest here.¹⁷ The resulting values of γ'_T and γ''_T with the 90%-confidence limit expressed as error bars are shown as the closed and open circles, respectively, in Fig. 3. Each set consisting of one open and one closed circle is determined from the concentration dependence of I^{s+p}/I^s at one value of ω_1 in either a CARS or a CSRS configuration.

The solid lines in Fig. 3 are a least-squares fit of the real and imaginary parts to the theoretical form of γ_T which we will now derive from the following expression:

$$\gamma_T = \left\langle \frac{A}{\omega_{gf} - 2\omega_1 - i\Gamma'_{gf}} \right\rangle, \quad (4)$$

where¹⁴

$$A = \frac{e^4 \Phi}{12\hbar^3} \left(\frac{x_{gi}x_{if}}{\omega_{gi} - \omega_1 - i\Gamma_{gi}} \right) \times \left(\frac{x_{gi}x_{if}}{\omega_{gi} - \omega_2 - i\Gamma_{gi}} + \frac{x_{gi}x_{if}}{\omega_{gi} - \omega_3 - i\Gamma_{gi}} \right). \quad (5)$$

ω_{gf} and Γ'_{gf} are the energy and width of the state accessible to two-photon excitation (only one such state is assumed for an individual chromophore). The ground state is represented by g and the final (two-photon) state by f . The bracket in Eq.

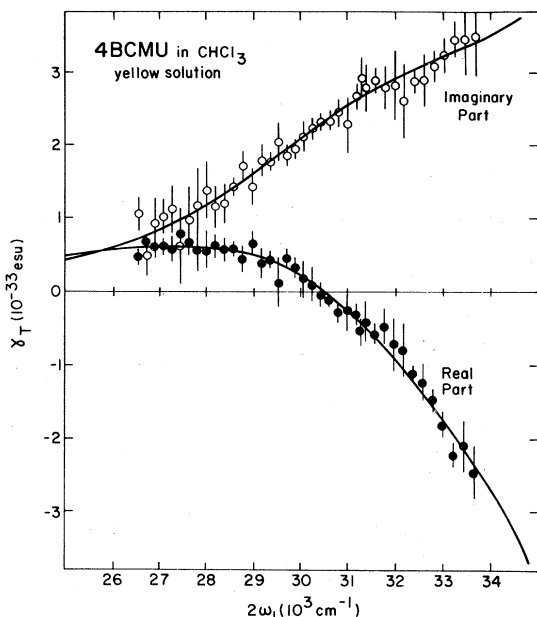


FIG. 3. Variation of the real (●) and imaginary (○) parts of the two-photon hyperpolarizability (γ_T) with two-photon energy ($2\omega_1$) for the yellow solution. The error bars represent 90% confidence limits. All data are taken in a 1111 geometry (all beams polarized \parallel). The solid lines are theoretical fits to the data according to Eq. (4).

(4) represents an average over the ensemble of chromophores interacting with the photon fields. Each molecule (or chromophore within a polymer molecule) has a slightly different set of parameters for the frequencies, intensities, and widths. The terms in parentheses in Eq. (5) represent the one-photon resonance enhancement to the two-photon absorption term in χ_T , with x_{jk} representing the transition moment between states j and k . It is assumed that one state (labeled i) with energy ω_{gi} and width Γ_{gi} is responsible for these resonances. The factor Φ accounts for the fact that the 3WM signal is an average over all molecular orientations in solution; Φ varies from 1 for an isotropic chromophore to $\frac{1}{5}$ for a one-dimensional chromophore.

In the experiments in the yellow solution, the energy differences $\omega_{gi} - \omega_n$ ($n=1, 2, 3$) are large compared to the width of any *single*-chromophore one-photon resonance (although not necessarily large compared to the distribution of energies which gives rise to the large inhomogeneous spectral widths in Fig. 1), so that Γ_{gi} can be neglected in A . In taking the average over chromophores in Eq. (4), we approximate A by its value found by substituting $\omega_{gi} = \langle \omega_{gi} \rangle = 21\,300\text{ cm}^{-1}$ from the one-photon absorption spectrum. (Note that $\langle \omega_{gi} \rangle$ is the same as E_0 discussed in Sec. I.) We also convert to oscillator strengths f_{jk} given by

$$f_{jk} = 2m \langle \omega_{jk} \rangle x_{jk}^2 / 3\hbar. \quad (6)$$

Thus, we have as the final form for the data analysis

$$\gamma_T \cong A / (\langle \omega_{gf} \rangle - 2\omega_1 - i\Gamma_{gf}), \quad (7)$$

where

$$A = \frac{3e^4 \Phi f_{gi} f_{if}}{16\hbar m^2 \langle \omega_{gi} \rangle \langle \omega_{if} \rangle} \left(\frac{1}{\langle \omega_{gi} \rangle - \omega_1} \right) \times \left(\frac{1}{\langle \omega_{gi} \rangle - \omega_2} + \frac{1}{\langle \omega_{gi} \rangle - \omega_3} \right). \quad (8)$$

The average over the ensemble of chromophores (i.e., chain lengths) has been approximated by a Lorentzian with a width Γ_{gf} which represents the inhomogeneous width of the two-photon resonance due to the distribution of chain lengths plus any vibrational progressions. The frequency $\langle \omega_{gi} \rangle$ and oscillator strength f_{gi} for the one-photon $g-i$ transition are obtained from linear absorption data such as those in Fig. 1. Therefore, the only parameters varied in the fitting procedure are $\langle \omega_{gf} \rangle$, Γ_{gf} (the average frequency and inhomogeneous width of the distribution of states accessible by two-photon absorption), and f_{if} the oscillator strength for the excitation from the intermediate state to the two-photon final state. Polarization measurements and theoretical calculations described later show that the state observed in linear absorption measurements is, as expected, the intermediate state in the two-photon resonance. For the theoretical curves of Fig. 3, values of Γ_{gi} from 0 to 100 cm^{-1} did not change the results. Larger values of Γ_{gi} did not give as good a fit to experiment.

The two-photon state as determined by the fit to the yellow-solution data has $\langle \omega_{gf} \rangle = 30\,500\text{ cm}^{-1}$. The effect of the one-photon resonance enhancement on γ_T can be seen if we consider the form of the solid curves in Fig. 3 under conditions that no one-photon resonance is present. In this case, γ_T' would be a dispersive-like curve with inversion symmetry around the $\gamma_T' = 0$ point at $30\,500\text{ cm}^{-1}$ and γ_T'' would be an absorptive-like curve centered at $30\,500\text{ cm}^{-1}$. The large increase in the magnitudes of γ_T' and γ_T'' on the high-energy side of the spectrum is therefore attributed to one-photon resonance. The peak expected for γ_T'' at $30\,500\text{ cm}^{-1}$ is barely discernible as a broad shoulder, since it is almost completely obscured by the one-photon resonance.

A test of the consistency of the data is that γ_T' / γ_T'' should be a straight line which crosses zero at $2\omega_1 = \omega_{gf}$ and with slope $= -1/\Gamma_{gf}$. Figure 4 shows the γ_T' / γ_T'' experimental points as circles and the theoretical straight line $(\langle \omega_{gf} \rangle - 2\omega_1) / \Gamma_{gf}$

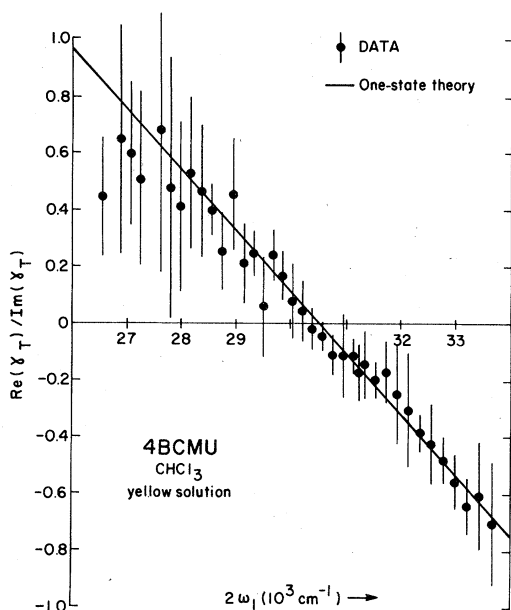


FIG. 4. Ratio of the real and imaginary parts of γ_T'' vs $2\omega_1$ for the yellow solution (Fig. 3 data). The straight line is the corresponding ratio for the theoretical curves of Fig. 3 (slope = $1/\Gamma_{gf}$; $2\omega_1$ intercept = $\langle\omega_{gf}\rangle$).

with the values of $\langle\omega_{gf}\rangle$ and Γ_{gf} previously determined. The consistency of the theoretical and experimental values indicates that the values of $\langle\omega_{gf}\rangle$ and Γ_{gf} are well determined.

The strong one-photon absorption is observed for polarization parallel to the chain axis.⁷ Polarization studies of the three-wave mixing demonstrate that the two-photon absorption observed in these experiments is also polarized along the chain axis. Table I shows the values of γ_T for two frequencies and for the two polarization configurations 1111 and 1221, where $ijji$ corresponds to ω_3 and ω_2 polarized along i and ω_1 polarized along j . Within experimental error $\gamma_T^{1111} = 3\gamma_T^{1221}$ and therefore $\chi_T^{1111} = 3\chi_T^{1221}$. The polarization of the intermediate state relative to the molecular chain axis can be determined by considering the relationship between the macroscopic term of the susceptibility labeled by the numbers 1 and 2 and the susceptibility in the molecule labeled by x , y , and z , where x is along the chain axis

TABLE I. Polarization studies in yellow solution (4BCMUs in CHCl_3).

Polarization	$2\omega_1$ (cm^{-1})	γ_T' (10^{-33} esu)	γ_T'' (10^{-33} esu)
1111	32362	-1.14 ± 0.11	2.95 ± 0.16
1221	32362	-0.32 ± 0.04	0.91 ± 0.04
1111	30581	0.11 ± 0.10	2.40 ± 0.13
1221	30581	0.04 ± 0.05	0.77 ± 0.04

and y is in the plane of the conjugated molecule. No electronic states accessible by z polarization are present in the molecule. Therefore, we have

$$\chi_T^{1111} = \frac{1}{15} [3\chi^{xxxx} + 3\chi^{yyyy} + 2(\chi^{xxyy} + \chi^{yyxx}) + (\chi^{xyyx} + \chi^{yxyx})] \quad (9)$$

and

$$\chi_T^{1221} = \frac{1}{15} [\chi^{xxxx} + \chi^{yyyy} - (\chi^{xxyy} + \chi^{yyxx}) + 2(\chi^{xyyx} + \chi^{yxyx})], \quad (10)$$

where all the χ 's in the molecule represent two-photon terms. The two polarizations which correspond to excitation of the two-photon state are the middle two (or outer two) in the $ijji$ notation. The two-photon state may be accessible by several combinations of the two photons in the molecular frame. These possibilities lead to the simplification of Eqs. (9) and (10) shown in Table II. The fact that $\chi^{1111}/\chi^{1221} = +3$ is inconsistent with crossed polarization having access to the two-photon state; crossed polarization requires $\chi^{1111}/\chi^{1221} = -2$. Whether χ^{yyyy} or χ^{xxxx} is the dominant term in the susceptibility cannot be determined solely from the polarization measurements. However, linear absorption measurements show that the allowed one-photon state is polarized along the chain axis (x axis) and, therefore, χ^{xxxx} is the dominant term. Thus, we have $\gamma_T^{1111} = \gamma_T^{xxxx}/5$ or $\Phi = \frac{1}{5}$ in Eq. (8). The symmetry assignments for the two-photon state can also be inferred as A_g , since the highly allowed one-photon transition is known to be $A_g \rightarrow B_u$ and, as we show later, the second step in the two-photon transition is also highly allowed ($B_u \rightarrow A_g$).

Similar measurements and analysis have been carried out for the red solution. In this case the concentration of polymer in the chloroform-hexane solvent is limited to less than 4×10^{17} r.u./ cm^3 . Therefore, the errors for γ_T' and γ_T'' are larger than in the case of the yellow solution. In addition, the absorption band of the red solution is shifted to the red with respect to that of the yellow solution. Therefore, $2\omega_1$ can only be extended up to $\sim 32000 \text{ cm}^{-1}$. The experimental values of γ_T' and γ_T'' and the theoretical curve

TABLE II. Correlation of macroscopic χ and microscopic χ for various assumptions of accessibility of two-photon state.

Two-photon polarizations	χ^{1111}	χ^{1221}
x, x	$(3\chi^{xxxx})/15$	$(\chi^{xxxx})/15$
x, y	$2(\chi^{xxyy} + \chi^{yyxx})/15$	$-(\chi^{xxyy} + \chi^{yyxx})/15$
y, y	$(3\chi^{yyyy})/15$	$(\chi^{yyyy})/15$

including all one-photon resonances are shown in Fig. 5. Although the errors are considerably larger for the data in Fig. 5 than that in Fig. 3, the determination of $\langle\omega_{gf}\rangle = 28\,100\text{ cm}^{-1}$ and $\Gamma_{gf} = 4000\text{ cm}^{-1}$ is reasonable and consistent with $\langle\omega_{gf}\rangle$ and Γ_{gf} for the yellow solution, as is shown later. Also, we have previously shown at selected frequencies that these γ_T values yield reasonably good fits to the Raman resonances in CARS experiments for both the red and the yellow solutions.

The blue solution, 3BCMU in chloroform and hexane, has similar linear optical properties to the 4BCMU red solution but with a considerable red shift of the linear absorption spectrum. Therefore, the accessible range of $2\omega_1$ is effectively limited to a single frequency ($26\,554\text{ cm}^{-1}$). The values of $\langle\omega_{gf}\rangle$ and Γ_{gf} have been determined in two ways. In the first case $\langle\omega_{gf}\rangle/\langle\omega_{gi}\rangle$ is assumed to be the same as in the yellow and red solutions (~ 1.46) which gives $\langle\omega_{gf}\rangle = 23\,200\text{ cm}^{-1}$. The value of $\gamma'_T/\gamma''_T = (\langle\omega_{gf}\rangle - 2\omega_1)/\Gamma_{gf}$ at $2\omega_1 = 26\,554\text{ cm}^{-1}$ then yields $\Gamma_{gf} = 2200\text{ cm}^{-1}$, and the amplitude of γ_T yields $f_{if} = 2.3$. In the second case Γ_{gf} is assumed to be 4000 cm^{-1} , as this is the maximum reasonable value of Γ_{gf} consistent with Γ_{gf} for the yellow and red solutions. Then γ'_T/γ''_T yields $\langle\omega_{gf}\rangle = 20\,500\text{ cm}^{-1}$ and the amplitude yields $f_{if} = 2.7$.

A comparison of the concentration dependence of the yellow solution and the blue solution at the

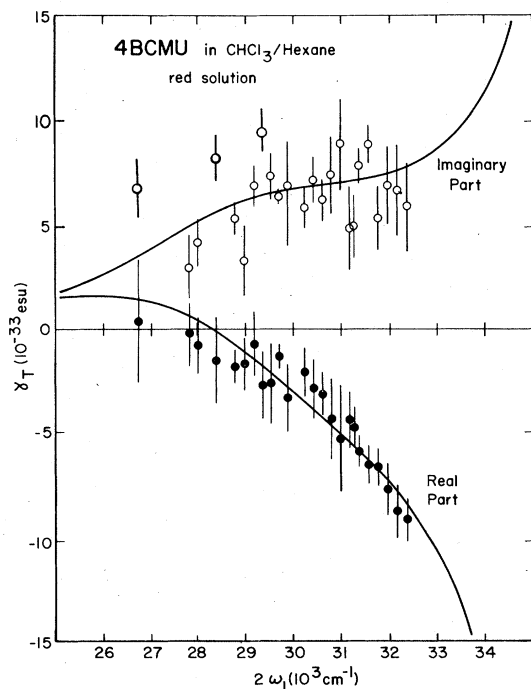


FIG. 5. Variation of the real (●) and imaginary (○) parts of γ_T vs $2\omega_1$ for the red solution.

same ω_1 such that $\langle\omega_{gf}\rangle$ (blue) $< 2\omega_1 < \langle\omega_{gf}\rangle$ (yellow) clearly shows the effect of the change of sign of γ'_T . This effect is shown in Fig. 6 for $2\omega_1 = 26\,554\text{ cm}^{-1}$.

The values $\langle\omega_{gf}\rangle$ and Γ_{gf} determined from the fitting to $\gamma_T(2\omega_1)$ from the red and yellow solutions along with $\langle\omega_{gf}\rangle$ and Γ_{gf} estimates for the blue solution are shown in Table III. The results for f_{gi} determined from linear absorption data and f_{if} determined from the γ_T data for all three solutions are also included in Table III. Note that these oscillator strengths correspond to the values appropriate for polarization parallel to the chain direction. Though the restricted data for the blue solution yields large uncertainties in the $\langle\omega_{gf}\rangle$ and Γ_{gf} values, f_{if} for the blue solution is reasonably well determined nevertheless.

It should be emphasized that the $\langle\omega_{gf}\rangle$ and Γ_{gf} values correspond to a Lorentzian description of the energy distribution of two-photon accessible states. The inhomogeneous width Γ_{gf} is attributed to a distribution of conjugation lengths plus vibrational sidebands. It is reasonable to expect this width to be similar to or somewhat greater

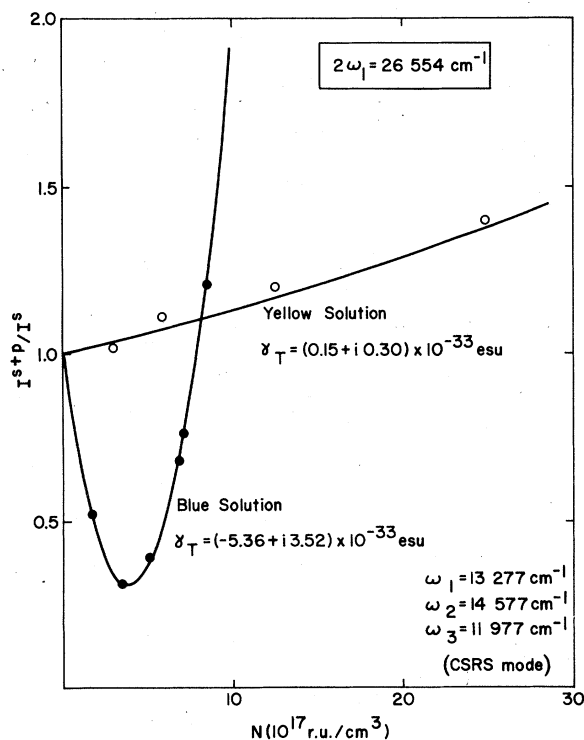


FIG. 6. Variation of the normalized ω_3 output intensity (CSRS) versus polymer concentration for the blue solution (●) and the yellow solution (○) at $2\omega_1 = 26\,554\text{ cm}^{-1}$. The solid lines are theoretical fits to the data: $\gamma_T = (0.15 + i0.30) \times 10^{-33}\text{ esu}$ for the yellow solution and $\gamma_T = (-5.36 + i3.52) \times 10^{-33}\text{ esu}$ for the blue solution.

TABLE III. Energies, widths, and oscillator strengths for one- and two-photon absorption in polydiacetylene solutions (energies and widths in cm^{-1}).

Solution	$\langle\omega_{gi}\rangle$	f_{gi}^a	$\langle\omega_{gf}\rangle$	Γ_{gf}	f_{if}^a
Yellow	21300	1.3	30500	4600	2.7
Red	18900	1.6	28100	4000	2.5
Blue	15900	1.4	{23200 20500}	{2200 4000}	{2.3 2.7}

^aBoth f_{gi} and f_{if} represent oscillator strengths for polarization parallel to the chain direction.

than the inhomogeneous width of the one-photon transition ($\sim 2500 \text{ cm}^{-1}$; see Fig. 1). As a consequence of this fitting procedure, $\langle\omega_{gf}\rangle$ represents an average energy for the two-photon state and the electronic origin (0-0 two-photon transition energy) would probably be less than $\langle\omega_{gf}\rangle$ by at most a few thousand wave numbers, i.e., $\sim \Gamma_{gf}$. This effect would be most important for the red and blue solutions where a fairly well defined 0-0 transition is evident in the solution spectra of Fig. 1. Thus, for the blue solution a near coincidence of ω_{gi} and ω_{gf} cannot be ruled out. These approximations in our estimate of ω_{gf} are of little consequence in the simplified theoretical discussion to follow and are ignored.

IV. THEORETICAL CONSIDERATIONS

In this section, we present a simple theoretical approach to the energy levels and the oscillator strengths for optical transitions between them. There have been several calculations of the energy levels of polydiacetylenes reported. Hückel-theory molecular-orbital (MO) models,²² extended Hückel models,²³ and exciton models²⁴ have been employed, but to our knowledge have not considered explicitly the chain-length dependence of the optical transitions. These calculations are analogous to the work on the polyenes, for which much more complete studies have been done. In order to describe the low-lying excited states of the polyenes, in particular the one-photon optical band gap, one can use a free-electron model,²⁵ a Hückel MO model²⁶ with bond alternation, or a Pariser-Parr-Pople π -electron calculation with configuration interaction (with or without bond alternation).²⁷ The one-photon gap has also been described using an exciton model.²⁸ In recent years, the low-lying g states have been the subject of a great deal of scrutiny, both experimental²⁹ and theoretical.³⁰ The lowest g state seems to be below the first optically allowed u state for large polyenes, and can be thought of as a double excitation state. Although there are

many similarities between the polyenes and polydiacetylenes, there are also many differences. For example, the polydiacetylenes have larger intrinsic bond alternation than the polyenes. In addition, many polyenes have been studied isolated in the gas phase, while all studies on polydiacetylenes are either in solid or solution phases.

In this section, we will describe the energy-level structure of the polydiacetylenes using Hückel molecular-orbital theory. This is clearly an oversimplified description; however, it has the advantage of being simple and giving surprisingly good results. It is our belief that a more sophisticated and accurate calculation is necessary in order to give a detailed understanding of the electronic transitions; however, no such calculation has been done to our knowledge. Our calculations are performed for both the acetylenic and butatrienic backbones, though it remains unclear whether or not a butatriene backbone is the best representation of the red solution polymer.¹³

The model is the standard Hückel theory: one π electron per carbon atom and nearest-neighbor one-electron integrals, $\beta(r)$, where r is the distance between the two neighboring atoms. The molecular orbitals for an N -carbon chain are calculated by diagonalizing the $N \times N$ one-electron matrix. (Note that $N=4n$, where n is the number of unit cells each containing 4 relevant carbon atoms.) The highest-occupied molecular orbital (HOMO) is number $N/2$ (number 1 is the lowest-energy orbital), the lowest unoccupied orbital is number $N/2+1$, and the next unoccupied orbital is number $N/2+2$. We will assume that the first optically allowed one-photon transition $g \rightarrow i$ is the excitation of an electron from $N/2$ to $N/2+1$, and that the first two-photon transition $g \rightarrow f$ is the excitation of an electron from $N/2$ to $N/2+2$ (or from $N/2-1$ to $N/2+1$, which has the same energy).

In order to perform the calculation, we must have a form for $\beta(r)$. Several forms have been suggested in the literature.²⁶ Our approach is semiempirical. We take

$$\beta(r) = C \exp(-\xi r) \quad (11)$$

and then find sets of values of C and ξ which, for $N \rightarrow \infty$, give the experimental one-photon band gap. The final choice of C and ξ was made by picking values that also gave β 's which were close to the values suggested in the literature. We used $C = 8.30 \times 10^5 \text{ cm}^{-1}$ and $\xi = 25.9 \text{ nm}^{-1}$.

We then diagonalized the one-electron matrix for values of N from $N=4$ to $N=40$, and found the energy of the one-photon transition (ω_{gi}) and the energy of the two-photon transition (ω_{gf}).

These values are fitted to smooth curves in Fig. 7 for the acetylenic and butatrienic forms of the polydiacetylenes. The geometries are taken from the x -ray data.⁵ We may also fit the one-photon optical transition ω_{gi} to a series in N^{-1} and find

$$\begin{aligned}\omega_{gi}^{\text{buta}} &= 7.1 \times 10^3 + 1 \times 10^5 N^{-1} \\ &+ 1.5 \times 10^4 N^{-2} \text{ cm}^{-1}, \\ \omega_{gi}^{\text{acet}} &= 1.5 \times 10^4 + 8.9 \times 10^4 N^{-1} \\ &+ 1.8 \times 10^4 N^{-2} \text{ cm}^{-1}.\end{aligned}\quad (12)$$

The two-photon energy gap found by this method is

$$\begin{aligned}\omega_{gf}^{\text{buta}} &= 7.3 \times 10^3 + 1.9 \times 10^5 N^{-1} \\ &+ 2.7 \times 10^5 N^{-2} \text{ cm}^{-1}, \\ \omega_{gf}^{\text{acet}} &= 1.5 \times 10^4 + 1.9 \times 10^5 N^{-1} \\ &+ 4.4 \times 10^4 N^{-2} \text{ cm}^{-1}.\end{aligned}\quad (13)$$

Experimentally, we find that $\omega_{gi}^{\text{acet}} \cong 16\,000 \text{ cm}^{-1}$ (assuming the blue solution to be the acetylenic form) and $\omega_{gi}^{\text{buta}} \cong 18\,900 \text{ cm}^{-1}$ (assuming the red solution to be the butatrienic form). This implies that in the butatrienic form N is between 8 and 12, while in the acetylenic form $N > 40$. The two-photon energy gap is found experimentally to be $\omega_{gf}^{\text{buta}} \cong 28\,000 \text{ cm}^{-1}$ and $\omega_{gf}^{\text{acet}} \cong 20\,200\text{--}23\,400 \text{ cm}^{-1}$, leading to N_{buta} between 8 and 12 again, and N_{acet} between 20 and 36. For the yellow solution,

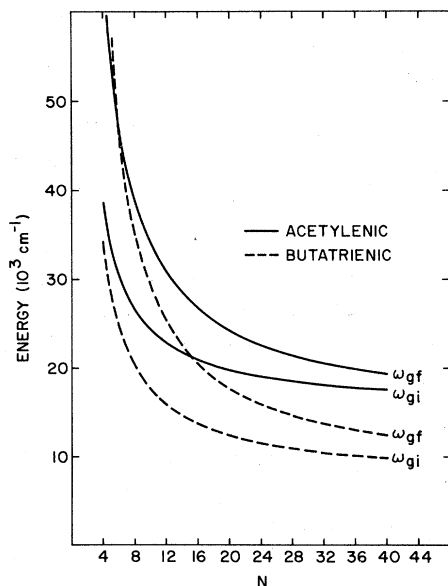


FIG. 7. Hückel-molecular-orbital-theory results for energies of two-photon and one-photon-allowed transitions as a function of number of carbon atoms in chain. (The number of polymer repeat units equals $N/4$.) Results are shown for both acetylenic and butatrienic backbones.

which we presume has an acetylene backbone, both the one- and two-photon transition energies are consistent with $N=12\text{--}16$ (which is identical to the estimate made from the degree of intramolecular hydrogen bonding in the substituent group¹²). Thus, the internal consistency of the model is reasonably good. Note, however, that these are very approximate results and the precise numbers should be given little weight.

If the red-solution results are interpreted within the acetylenic model, ω_{gi} requires $N=24\text{--}28$ while ω_{gf} requires $N=12\text{--}16$. Thus, our red-solution results are more consistent with the butatrienic backbone. However, as pointed out previously, intramolecular hydrogen bonding between the urethane substituent groups for the 4BCMU polymer results in a strain on the backbone. Thus, the supporting evidence for the butatriene-backbone conformation, including this work, could be a fortuitous consequence of the backbone distortion induced by an intramolecular strain field.¹³ Also, as mentioned previously, ω_{gf} would tend to be overestimated by our treatment of the experimental data.

We turn now to the calculation of oscillator strengths in this model. We assume that the one-photon oscillator strength is just that for the transition $N/2$ to $N/2+1$. We further assume that the oscillator strengths for the two-photon absorption are (1) from $N/2$ to $N/2+1$ and (2) from $N/2+1$ to $N/2+2$. This approach neglects the configuration mixing which will occur in the g states, but we expect this approximation to be qualitatively accurate. We compute the transition moments (from $N/2 \rightarrow N/2+1$ and from $N/2+1 \rightarrow N/2+2$) by neglecting differential overlap so that, for example,

TABLE IV. Transition moments from theoretical model. Values of α given have not been normalized by number of carbon atoms in chain (N).

N	$x_{gi}(\theta)^a$	$x_{if}(\theta)$
Acetylenic structure		
8	1.5 (9°)	2.2 (0°)
16	2.3 (5°)	4.3 (0°)
24	2.7 (4°)	6.3 (-1°)
40	3.2 (3°)	10.0 (-1°)
Butatrienic structure		
8	1.7 (12°)	2.2 (0°)
12	2.4 (8°)	3.3 (0°)
16	2.9 (7°)	4.3 (0°)
32	4.4 (4°)	8.3 (0°)

^aThe number in parentheses is the calculated angle between the transition moment and the chain direction.

TABLE V. Relative oscillator strengths from theoretical model.

Acetylenic form		Butatrienic form	
N	f_{gi}/f_{if}	N	f_{gi}/f_{if}
8	1.2	8	1.1
16	1.1	12	0.9
24	1.0	16	1.0
40	1.0	32	0.9

$$\begin{aligned} \langle \phi_{N/2} | \vec{r} | \phi_{N/2+1} \rangle &= \sum_{i \neq j} C_i^{N/2} C_j^{N/2+1} \langle u_i | \vec{r} | u_j \rangle \\ &= \sum_i C_i^{N/2} C_i^{N/2+1} \langle u_i | \vec{r} | u_i \rangle, \quad (14) \end{aligned}$$

where ϕ_k is the k th molecular orbital, u_i is the atomic p_x orbital on site i , and C_i^k is the coefficient of the i th atomic orbital in the k th molecular orbital. By assuming

$$\langle u_i | \vec{r} | u_i \rangle = \vec{r}_i$$

we can reduce the transition moment to a simple sum. Using the geometries of the molecules from the x -ray structures and the coefficients from our energy calculations, we compute the relevant transition moments. They are given in Table IV for both transitions and both structures for a number of N values. In addition, we have calculated the angle the transition moment makes with the long axis of the molecule, and this is also given in Table IV. In Table V, we give the relative oscillator strengths for the $g \rightarrow i$ transition with respect to the $i \rightarrow f$ transition.

A number of comments should be made about these results. First, the transition $N/2 + 1 \rightarrow N/2 + 2$ lies within 1° of the long axis of the molecule while the transition $N/2 \rightarrow N/2 + 1$ is about 4° off the long axis for both structures for large N and is farther from the axis for small N . Second, the relative oscillator strengths are approximately 1 for all N ; thus, the "second step" in the two-photon absorption is as allowed as the first step for all N considered, in complete agreement with experimental results.

V. DISCUSSION

The internal consistency of results for the three polymer solutions and the good agreement between theory and experiment described above strongly suggest that the large two-photon hyperpolarizability is a general property of polydiacetylenes. The origin of the large γ_T values is a combination of large oscillator strengths and large one-photon resonance effects. Polydiacetylene crystals,

which have $\omega_{gi} = 15\,000$ – $19\,000$ cm^{-1} , should also display large two-photon absorption TPA. This is an important point if these materials are to be considered for use in nonlinear optical devices based on the large susceptibilities measured with infrared lasers.¹

There have been two previous measurements of TPA in polydiacetylene crystals. Reimer and Bässler³¹ found a two-photon absorption coefficient, β , of $\sim 5 \times 10^{-48}$ $\text{cm}^4 \text{sec}/\text{photon r.u.}$ at $2\omega = 18\,880$ cm^{-1} for PTS (R in polydiacetylene structure is $-\text{CH}_2\text{SO}_3\text{C}_6\text{H}_4\text{CH}_3$; $\langle \omega_{gi} \rangle = 16\,200$ cm^{-1}). This value is large, though not remarkably so. β can be derived from our measurements as

$$\begin{aligned} \beta &= \frac{9\pi^2 e^4 f_{gi} f_{if} (2\omega)^2}{4n^2 C^2 m^2 \langle \omega_{gi} \rangle \langle \omega_{if} \rangle} \left(\frac{1}{\langle \omega_{gi} \rangle - \omega_p} + \frac{1}{\langle \omega_{gi} \rangle - \omega_x} \right) \\ &\quad \times G(2\omega - \omega_{gf}), \quad (15) \end{aligned}$$

where

$$G(2\omega - \omega_{gf}) = \Gamma_{gf} / [(\langle \omega_{gf} \rangle - 2\omega)^2 + \Gamma_{gf}^2]. \quad (16)$$

The frequencies ω_x and ω_p ($2\omega = \omega_x + \omega_p$) are the excitation frequencies. In the Reimer and Bässler experiment $\omega_x = \omega_p = 9440$ cm^{-1} . The above β is related to the hyperpolarizability by

$$\beta = \frac{60\pi h (2\omega)^2}{n^2 C^2} \text{Im}(\gamma_T^{xxxx}). \quad (17)$$

The γ_T term in this equation is $\gamma_T(-\omega_x, \omega_x, \omega_p, -\omega_p)$ compared to $\gamma_T(-\omega_3, \omega_1, \omega_1, -\omega_2)$ measured here. The only difference is the form of the one-photon resonance terms [see Eq. (8)].

Lequime and Hermann¹³ measured TPA over an extended range in two polymers: PTS and TCDU [R is $-(\text{CH}_2)_4 \text{OCONHC}_6\text{H}_5$; $\langle \omega_{gi} \rangle = 18\,500$ cm^{-1}]. They utilized a 9440 - cm^{-1} excitation beam (ω_x) and a low-intensity probe beam (ω_p). Their results, shown in Fig. 8, are in good agreement with the single-frequency result of Ref. 31 and indicate remarkably large β values, especially for PTS. They attributed this absorption to a two-step process involving defect formation and defect absorption. The solid lines in Fig. 8 represent fits of Eq. (15) to their data with $f_{gi} f_{if}$ as an adjustable parameter and other TPA parameters in Eq. (15) estimated as follows: PTS, $\langle \omega_{gf} \rangle = 22\,000$ cm^{-1} and $\Gamma_{gf} = 3000$ cm^{-1} , and TCDU, $\langle \omega_{gf} \rangle = 27\,500$ cm^{-1} and $\Gamma_{gf} = 4000$ cm^{-1} . We find $f_{gi} f_{if} = 1.5$ for PTS and $f_{gi} f_{if} = 3.0$ for TCDU. The one-photon oscillator strengths f_{gi} have not been determined accurately for either of these materials but are on the order of unity. Therefore, the f_{if} values are in quite reasonable agreement with our solution results. We conclude that the data of Lequime of Hermann, including the large difference between PTS and

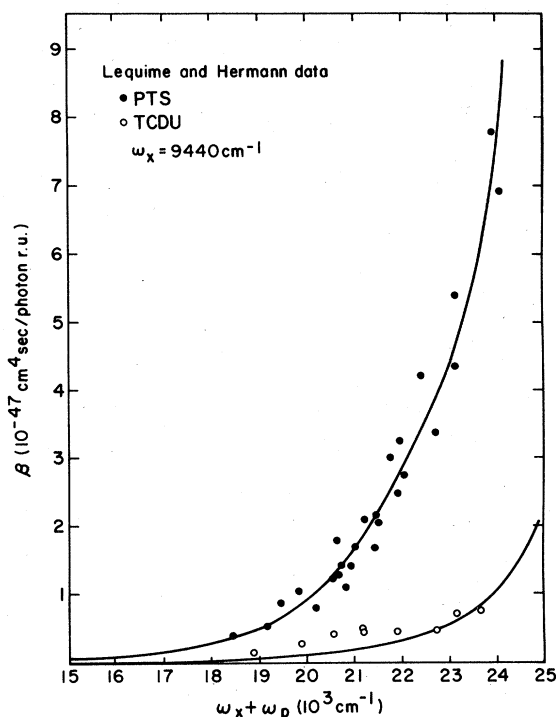


FIG. 8. Two-photon absorption coefficient versus two-photon energy ($\omega_x + \omega_p$) for two polydiacetylene crystals. Experimental data are from Lequime and Hermann and are taken with both beams parallel to the polymer chain direction. The solid lines are theoretical fits to the data according to Eq. (14).

TCDU, are easily explained by TPA without invoking defects. We further conclude that strong TPA is a fundamental property of the polydiacetylene backbone.

The large values of the hyperpolarizability in these molecules imply large susceptibilities for more concentrated solutions or solid-state films. This large susceptibility can be utilized in a para-

metric oscillator, even though χ has its origin in two-photon absorption.³² Linear absorption limits these devices to energies below 600 nm in 4BCMU, for example. This energy range is appropriate for extending the output of the alexandrite laser which produces line emission at 680 nm and tunable emission from 700 to 820 nm.³³ 3WM leads to generation of light with wavelengths as long as 1.1 μm . The efficiency of converting 680-nm radiation to the ir for an oriented film of 4BCMU is calculated to be 1–10% depending on incident intensities. TPA limits the intensity of the incident beams which may be used.

Two experiments were attempted with higher density polymer materials. CSRS was observed in 4BCMU single crystal, $\sim 69 \mu\text{m}$ thick, with $\omega_1 = 730 \text{ nm}$. Very little energy ($\sim 1.8 \mu\text{J}$) focused on the sample caused visible change; the sample turned red, presumably due to melting and conjugation length shortening.⁷ In a second experiment CARS was observed in a 4BCMU gel³⁴ with a density of $\sim 10^{18} \text{ r.u./cm}^3$. The incident beam at $\omega_1 = 650 \text{ nm}$ was not absorbed and no damage occurred. However, the CARS signal was strongly dependent on position of focusing in the sample due to inhomogeneities in the gel and was not as large as predicted from solution measurements. Therefore, these polymers are not at present practical parametric oscillators because of limitations of sample quality and, possibly, of TPA.

ACKNOWLEDGMENTS

We thank J. M. Sowa and M. C. Baker for technical assistance, G. N. Patel for supplying the polymer materials, and the National Science Foundation (Grant No. DMR-7908307) for partial support of this work. Helpful discussions with J. P. Hermann are also gratefully acknowledged.

¹C. Sauteret, J. Hermann, R. Frey, F. Pradère, J. Ducuing, R. H. Baughman, and R. R. Chance, *Phys. Rev. Lett.* **36**, 956 (1976).

²H. Eckhardt, C. J. Eckhardt, and K. C. Yee, *J. Chem. Phys.* **70**, 5498 (1979).

³R. R. Chance, R. H. Baughman, H. Müller, and C. J. Eckhardt, *J. Chem. Phys.* **67**, 3616 (1977).

⁴See, for example, D. Bloor, D. A. Fisher, D. N. Batchelder, R. Kennedy, A. C. Cottle, and W. F. Lewis, *Mol. Cryst. Liq. Cryst.* **52**, 83 (1979).

⁵V. Enkelmann and J. B. Lando, *Acta Crystallogr. B* **34**, 2352 (1978).

⁶Z. Iqbal, R. R. Chance, and R. H. Baughman, *J. Chem. Phys.* **66**, 5520 (1977).

⁷R. R. Chance, G. N. Patel, and J. D. Witt, *J. Chem. Phys.* **71**, 206 (1979).

⁸See, for example, H. Shirakawa, T. Ito, and S. Ikeda, *Polym. J.* **4**, 460 (1973).

⁹R. H. Baughman and R. R. Chance, *J. Polym. Sci., Polym. Phys. Ed.* **14**, 2037 (1976).

¹⁰J. Ducuing (private communication).

¹¹M. Lequime and J. Hermann, *Chem. Phys.* **26**, 431 (1977).

¹²G. N. Patel, R. R. Chance, and J. D. Witt, *J. Chem. Phys.* **70**, 4387 (1979).

¹³R. R. Chance, *Macromolecules* **13**, 396 (1980).

¹⁴M. D. Levenson and N. Bloembergen, *Phys. Rev. B* **10**, 447 (1974).

¹⁵H. Lotem and R. T. Lynch, *Phys. Rev. Lett.* **37**, 334 (1976).

¹⁶R. T. Lynch, S. O. Kramer, H. Lotem, and N. Bloembergen, *Opt. Commun.* **16**, 372 (1976).

- ¹⁷H. Lotem, R. T. Lynch, and N. Bloembergen, *Phys. Rev. A* **14**, 1748 (1976).
- ¹⁸R. T. Lynch and H. Lotem, *J. Chem. Phys.* **66**, 1905 (1977).
- ¹⁹R. M. Hochstrasser, G. R. Meredith, and H. P. Trommsdorff, *Chem. Phys. Lett.* **53**, 423 (1978).
- ²⁰M. L. Shand, R. R. Chance, and R. J. Silbey, *Chem. Phys. Lett.* **64**, 448 (1979).
- ²¹M. L. Shand and R. R. Chance, *J. Chem. Phys.* **71**, 4482 (1978).
- ²²E. G. Wilson, *J. Phys. C* **8**, 727 (1975); C. Cojan, G. P. Agrawal, and C. Flytzanis, *Phys. Rev. B* **15**, 909 (1977).
- ²³M. H. Whangbo, R. Hoffmann, and R. B. Woodward, *Proc. R. Soc. London A* **366**, 23 (1979).
- ²⁴M. Philpott, *Chem. Phys. Lett.* **50**, 18 (1977); D. Yarkony, *Chem. Phys.* **33**, 171 (1978).
- ²⁵H. Kuhn, *J. Chem. Phys.* **17**, 1198 (1949).
- ²⁶L. Salem, *Molecular Orbital Theory of Conjugated Systems* (Benjamin, New York, 1966).
- ²⁷L. Johnston and T. Peacock, *Mol. Phys.* **20**, 849 (1971).
- ²⁸J. Pople and S. Walmsley, *Trans. Faraday Soc.* **58**, 441 (1962).
- ²⁹B. Hudson and B. Kohler, *Annu. Rev. Phys. Chem.* **25**, 437 (1974).
- ³⁰K. Schulten and M. Karplus, *Chem. Phys. Lett.* **14**, 305 (1972); K. Schulten, I. Ohmine, and M. Karplus, *J. Chem. Phys.* **64**, 4422 (1976).
- ³¹B. Reimer and H. Bässler, *Chem. Phys. Lett.* **55**, 315 (1978).
- ³²L. B. Meisner and N. G. Khadziiski, *Kvant. Elektron. (Moscow)* **6**, 345 (1979) [*Sov. J. Quantum Electron.* **9**, 199 (1979)].
- ³³J. C. Walling, O. G. Peterson, and R. C. Morris, *IEEE J. Quantum Electron.* **16**, 120 (1980).
- ³⁴G. N. Patel and Y. P. Khanna, *J. Polym. Sci., Polym. Phys. Ed.* (in press).